Sustainable Materials and Technologies 46 (2025) e01703

Contents lists available at ScienceDirect

Sustainable Materials and Technologies

journal homepage: www.elsevier.com/locate/susmat

A facile approach for eco-friendly and low-cost triphenylamine-containing poly(vinyl acetal) with electrochromism/electrofluorochromism

Yu-Jen Shao [a,b,1], Chin-Hsuan Lin [a,2], Toshifumi Satoh [c,d,e,*], Cha-Wen Chang [f,**], Guey-Sheng Liou [a,**]

[a] Institute of Polymer Science and Engineering, National Taiwan University, 1 Roosevelt Road, 4th Sec., Taipei 106319, Taiwan
[b] Graduate School of Chemical Sciences and Engineering, Hokkaido University, Kita 13 Nishi 8, Sapporo 060-8628, Hokkaido, Japan
[c] Division of Applied Chemistry, Faculty of Engineering, Hokkaido University, Kita 13 Nishi 8, Sapporo 060-8628, Hokkaido, Japan
[d] List Sustainable Digital Transformation Catalyst Collaboration Research Platform (List-PF), Institute for Chemical Reaction Design and Discovery (ICReDD), Hokkaido University, Kita 13 Nishi 8, Sapporo 001-0021, Hokkaido, Japan
[e] Department of Chemical and Materials Engineering, National Central University, No. 300, Zhongda Rd., Zhongli Dist., Taoyuan 320317, Taiwan
[f] Department of Digital Printing Materials, Division of Applied Chemistry, Material and Chemical Research Laboratories, Industrial Technology Research Institute, 321 Kuang Fu Road, 2nd Sec., Hsinchu 300044, Taiwan

ARTICLE INFO

Keywords:
Poly(vinyl alcohol)
Triphenylamine
Poly(vinyl acetal)
Electrochromism
Electrofluorochromism

ABSTRACT

In this work, the low-cost and highly transparent poly(vinyl alcohol) (PVA) is utilized as the starting polymer to react with the 4-formyltriphenylamine (TPA) via acetalization reaction, preparing TPA-containing poly(vinyl acetal) (PVA-TPA). After casting on the ITO-coated glass and undergoing an electrochemical coupling reaction, the resulting cross-linking polymer (c-PVA-TPA) still exhibits high transparency and colorless appearance in the neutral state, which is beneficial for electrochromic applications. The cross-linking c-PVA-TPA electrochromic electrode exhibited an orange-brown and navy-blue appearance in the first and second oxidation stages, with quick response capability in the bleaching process in the first and second stages of only 1.2 s and 1.5 s, respectively. Furthermore, the gel-type electrochromic devices (ECD) of c-PVA-TPA also revealed prompt switching behavior, with t_c and t_b of 1.7 s and 2.0 s, respectively, and a coloration efficiency of about 360.5 cm^2 C^{-1}, which is superior to the structure-related electrochromic polyamide (TPB-PA). Furthermore, it also demonstrated electrofluorochromic characteristics by a 34.6-fold contrast ratio.

1. Introduction

Electrochromism (EC) is an attractive research and application to the world because it is an absorption-mode display that would not cause damage to our naked eyes [1]. Owing to the no light stimuli in EC displays, plenty of researchers focus on the development of versatile materials to develop and improve the EC properties, such as small organics (viologens) [2–4], inorganics (WO_3 and VO_x) [5], metal complexes (Prussian blue) [6–8], and conjugated polymers (PEDOT and PANI) [9–11]. Triphenylamine (TPA), a well-recognized fourth-generation EC material, is a widely used molecular architecture in designing versatile small molecules or polymers owing to their low oxidation potential, redox reversibility, and tunable color change by introducing specific counterparts or functional groups [1,12]. Furthermore, depending on the different π-bridge length or structure between two or more electroactive nitrogen centers, the formation of the intervalence charge transfer (IVCT) would result in the NIR wavelength absorption when partially oxidized by the electronic coupling between oxidized and non-oxidizzed electroactive centers [13,14]. To achieve this unique optical modulation, complex molecular design and synthesis are essential. Typically, high temperatures, precious metal-catalyzed (such as $Pd(OAc)_2$ and $Pd_2(dba)_3$), or expensive ligands (such as X-Phos and P*t*-Bu_3) are employed to synthesize the well-designed electrochromic molecules or monomers (Scheme 1). For polymeric EC materials, further

* Corresponding author at: Division of Applied Chemistry, Faculty of Engineering, Hokkaido University, Kita 13 Nishi 8, Sapporo 060-8628, Hokkaido, Japan.
** Corresponding authors.
E-mail addresses: satoh@eng.hokudai.ac.jp (T. Satoh), ChaWen@itri.org.tw (C.-W. Chang), gsliou@ntu.edu.tw (G.-S. Liou).
[1] Institute of Polymer Science and Engineering, National Taiwan University, 1 Roosevelt Road, 4th Sec., Taipei 106319, Taiwan; Graduate School of Chemical Sciences and Engineering, Hokkaido University, Kita 13 Nishi 8, Sapporo 060–8628, Hokkaido, Japan.
[2] Institute of Polymer Science and Engineering, National Taiwan University, 1 Roosevelt Road, 4th Sec., Taipei 106319, Taiwan.

https://doi.org/10.1016/j.susmat.2025.e01703
Received 23 July 2025; Received in revised form 1 September 2025; Accepted 6 October 2025
Available online 16 October 2025

polymerization processes, such as polycondensation or electrodeposition, are necessary to acquire the derived polymers subsequently. For example, polyamide EC materials usually exhibit a colorless appearance in the neutral state to achieve the gratifying colorless-to-color EC feature; however, the target TPA-based monomers and polymers also need complicated synthesis procedures, utilize expensive chemicals, and sometimes require high polymerization temperatures. Although the electrodeposition method could make the EC materials generate an intrinsic mesoporous conformation, which is beneficial to the diffusivity of the counter ions, quite a percentage of the starting materials would be wasted in preparing the EC electrode. Besides, the resulting conjugated polymer films usually reveal an inevitable drawback of accompanying dense color in the neutral state. Therefore, it is imperative to streamline complex synthesis pathways and design and develop a cost-effective, scalable, straightforward preparation strategy, yet the resulting redox-active materials perform remarkable EC behaviors. In a complete assembly EC device, the working electrode (electrochromic layer) operates in tandem with a counter electrode that provides the complementary redox (charge-balancing) reaction [1,15]. Viologens are frequently employed as cathodically supplemental counterparts to broaden the color range and enhance electrochemical stability in the TPA-based EC materials [16]. Between these electrodes is an electrolyte that supplies counter ions and ensures ionic conductivity while remaining electronically insulating. Liquid electrolytes offer high ionic conductivity and rapid switching but pose challenges in leakage, encapsulation, and long-term dimensional stability. Gel electrolytes reduce leakage, improve mechanical integrity, and enable flexible or laminated form factors.

Poly(vinyl alcohol) (PVA) is a well-commercialized polymer with a competitive price (*c.a.* $1.61/kg) that has widely gained significant attention due to its unique characteristics, including excellent film-formability and adhesion, high biocompatibility, and water-soluble

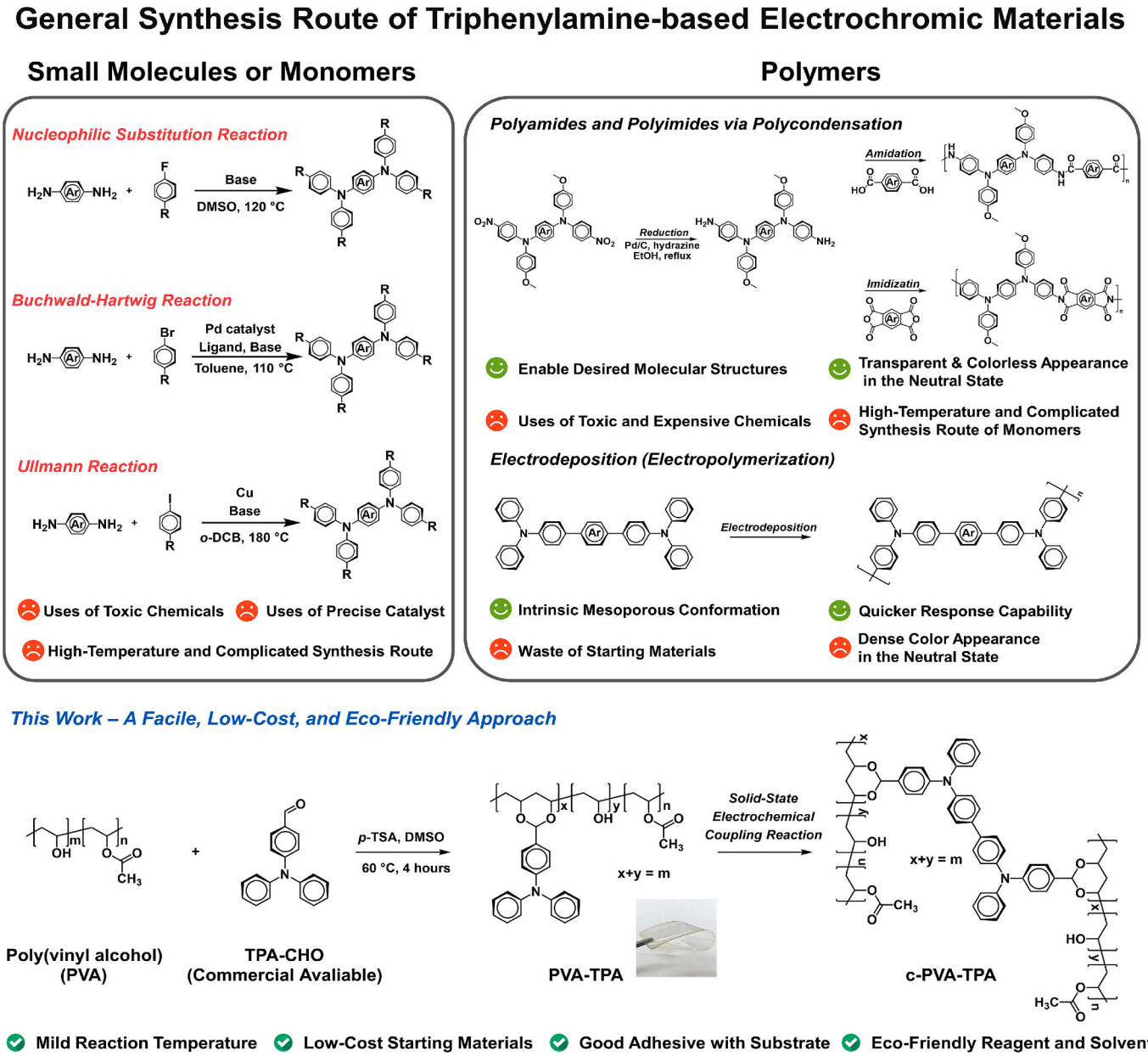

Scheme 1. General synthesis routes of the conventional triphenylamine-based electrochromic materials and the comparison with this work.

properties owing to the numerous hydroxyl groups (-OH) along its backbone [17,18]. PVA is generally synthesized through the hydrolysis of polyvinyl acetate (PVAc), and the hydrolysis degree could be tuned to produce PVA with varying properties. As the hydroxyl groups on its backbone, PVA offers remarkable opportunities for modification and functionalization, making it particularly valuable in various electrochemical systems, such as an electrode modifier [19–21], separator material [22–25], and binding agent [26–29]. Besides, PVA can be further processed to produce polyvinyl acetal with various aldehyde-containing compounds to undergo acetalization reaction, such as polyvinyl butyral (PVB) and polyvinyl formal (PVF) [30,31]. The resulting polyvinyl acetals can preserve high transparency and strong bonding strength with many materials, coupled with their excellent optical and mechanical properties, making them pivotal in automotive and construction as a laminated interlayer material [32–34]. Recently, polyvinyl acetals have expanded their ability to be applied in electrochemical processes as polymer electrolytes [35–39]. Yang and Song et al. developed a solid polymer electrolyte (SPE) for EC devices via cross-linking reaction of PVB with 3-glycidoxypropyltrimethoxysilane (KH560) to play as a safety glass layer with a highly transparent feature simultaneously, and the ionic conductivity of the resulting electrolyte reached 1.51×10^{-4} S cm^{-1} [35]. Wang et al. prepared PVB-based SPE by adding silica as an additive, and it could achieve an ionic conductivity as high as 1.78×10^{-4} S cm^{-1} [36]. To our knowledge, few researchers utilize redox-active poly(vinyl acetal) structures in electrochemical or EC applications as the working electrode. Hence, the motif of this work endeavors to develop low-cost TPA-based EC material, reduce the synthetic process, and limit toxic synthetic starting materials and catalysts to achieve eco-friendly features. Herein, PVA was chosen to be the base polymer and modified by the commercially available 4-formyltriphenylamine to undergo acetalization utilizing *p*-toluenesulfonic acid monohydrate (*p*-TSA) as the eco-friendly, non-toxic catalyst and dimethyl sulfoxide (DMSO) as a less-toxic and green solvent to obtain TPA-containing poly(vinyl acetal) (PVA-TPA) [40–42]. This approach could substantially reduce the synthetic procedures and toxic and environmentally harmful chemicals, and only requires a mild reaction temperature of 60 °C (Scheme 1). A following solid-state electrochemical coupling reaction on PVA-TPA film was conducted to form the cross-linked type EC material, c-PVA-TPA, which exhibits comparable properties to the structure-related conventional tetraphenylbenzidine (TPB)-based EC polyamide (TPB-PA). This result implies the promise of this facile, eco-friendly, and low-cost material as an up-and-coming candidate for practical use, such as a smart automotive window, as a laminated interlayer EC material.

2. Results and discussions

2.1. Synthesis, characterization, and the basic properties of PVA-TPA

TPA-PVA was prepared by the commercially available PVA (BP-17, M_w: 84,000–89,000; hydrolysis degree: 86% ~ 89%) and 4-formyltriphenylamine at a mild reaction temperature of 60 °C for four hours with DMSO and *p*-TSA as the solvent and catalyst, respectively. This approach simplified and mitigated synthetic routes and reaction temperature, reducing toxic and expensive chemicals. To characterize the acetalization degree of PVA-TPA, it is necessary first to calculate the actual hydrolysis degree of the commercialized PVA. In the ^{1}H NMR spectrum (Fig. S1), the 1.22 to 1.55 ppm signals are assigned to the PVA backbone's methylene group (–CH_2–) with an integral value of 1.0, and the signals from 1.89 to 2.02 ppm are the methyl group of the side-chain acetate group (–$OCOCH_3$) with an integral value of 0.22. Hence, the hydrolysis degree of the PVA used in this study could be estimated as 0.85. Next, the acetalization of the TPA-functionalized polyvinyl acetal could be calculated using the following equation:

$$Acetalization\ (\%) = \frac{S_{H\ of\ acetal} \times 4}{S_{1.10\ to\ 2.00\ ppm} \times 0.82 \times 0.85}$$

Where *S* is the integral area value, 0.85 is the hydrolysis degree, and 0.82 is the integral ratio of methylene groups in the PVA backbone and the methyl group of the side-chain acetate. In Fig. 1, the signals from 1.10 to 2.00 ppm were assigned to the polymer backbone's methylene groups and the methyl groups of the side-chain acetate, and the proton signal at 5.44 ppm was ascribed to the acetal's proton. According to the equation, the degree of acetalization could be estimated to be 63.3%, and it is not easy to achieve a complete or high acetalization degree because the acetalization reaction is reversible [41]. Therefore, an acetalization degree of 63.3% is considered a good level of functionalization. Besides, after the acetalization reaction, the FTIR spectra also revealed that the hydroxyl peak of PVA at 3304 cm^{-1} would be weakened, and the characteristic C-O-C peak of acetal would generate at 1107 cm^{-1}, as shown in Fig. S2. The resulting PVA-TPA revealed enhanced solubility in the common organic solvents, such as 1,4-dioxane, tetrahydrofuran (THF), dimethylformamide (DMF), dimethyl sulfoxide (DMSO), and dimethylacetamide (DMAc), as tabulated in Table S1, compared with the pristine PVA, which usually could dissolve only in THF, DMSO, and water. Besides, the PVA-TPA exhibited higher thermal stability than the pristine PVA, which manifested higher 5 wt% and 10 wt% mass loss temperatures (T_d [5] and T_d [10]) of 325 and 330 °C, respectively (Fig. S3 and Table S2). Due to incorporating aromatic moieties in the polymer structure, the glass transition temperature (T_g) of PVA-TPA could be increased to 137 °C, while the pristine PVA revealed a T_g of 78 °C (Fig. S4). Some references also reported the same trend: using aromatic or bulky moieties, the T_g would increase after acetalization [43,44]. In the mechanical test shown in Fig. S5, although PVA-TPA would show a larger Young's modulus (1033.5 MPa) than the pristine PVA (822.7 MPa), it would exhibit a brittle feature, with the elongation at break being only 4.5%.

To analyze the cost-effectiveness of PVA-TPA, we compared a structure-related TPB-based polyamide (TPB-PA), as shown in Scheme 1. All the unit prices of the chemicals were obtained from CAS SciFinder. According to the reference, we can approximate and evaluate the cost of the conventional TPB-PA, and the synthesis route is depicted in Scheme S1 [45,46]. As tabulated in Table S3, the starting diamine monomer (TPB-2NH_2) for TPB-PA had an extremely high cost of 211,000 USD/kg, leading to a high price to produce one kilogram of TPB-PA with 150,415 USD/kg. In contrast, PVA-TPA only required 716 USD to produce one kilogram of the product. We also listed the toxicity assessment of the solvents and chemicals used, and the chemicals used in this work had lower toxicity than those used to produce TPB-PA (Table S4). Therefore, PVA-TPA revealed a promising, low-cost, and eco-friendly EC material.

2.2. Observation of the electrochemical coupling reaction

To undergo the solid-state electrochemical coupling reaction, the PVA-TPA polymer film was drop-coated on the ITO-coated glass with a thickness of ca. 350 nm, as depicted in Fig. S6. At the first cycle of the cyclic voltammetry (CV), PVA-TPA did not show a prominent oxidation peak as the potential increased to 1.20 V, while two corresponding reduction peaks were observed at 0.72 V and 0.61 V in the reverse scan, as illustrated in Fig. 2a. At the second CV scan, the onset oxidation potential ($E_{ox,\ onset}$) was decreased from 0.87 V to 0.68 V, implying that the benzidine moiety was formed via the electrochemical coupling reaction and increased the highest occupied molecular orbital (HOMO) level from −5.23 eV to −5.04 eV (vs. Fc/Fc$^+$, $E_{ox,\ onset}$ = 0.44 V); and two new oxidation potentials generated as observed at 0.87 V and 1.16 V. This phenomenon is the same as the electrodeposition method to prepare polymeric EC materials, where the occurrence of the lower $E_{ox,\ onset}$ and the generation of new oxidation peaks typically accompany the coupling reaction [47,48]. In the differential pulse voltammetry (DPV), similar

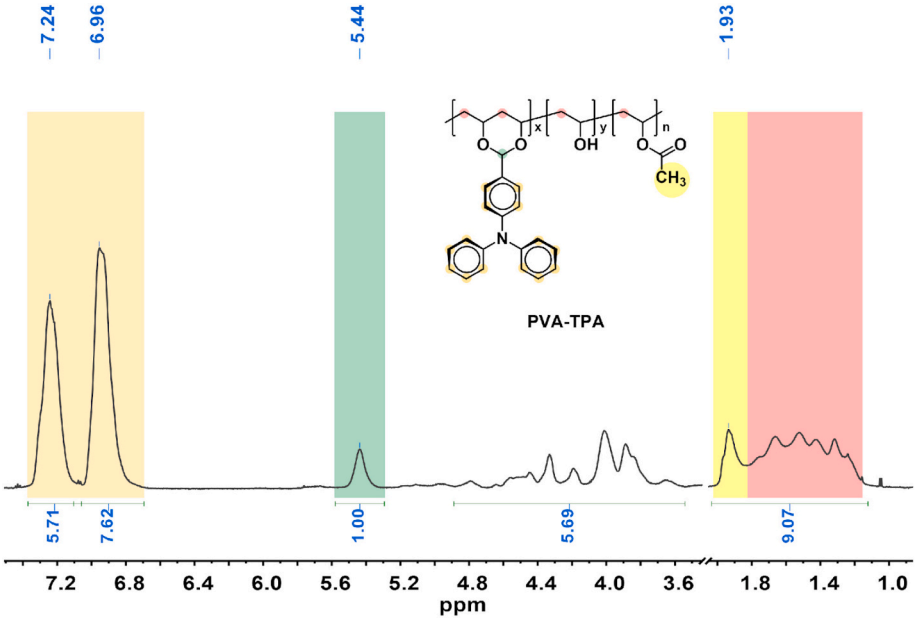

Fig. 1. ^{1}H NMR spectrum of PVA-TPA in DMSO-d_6. (600 MHz).

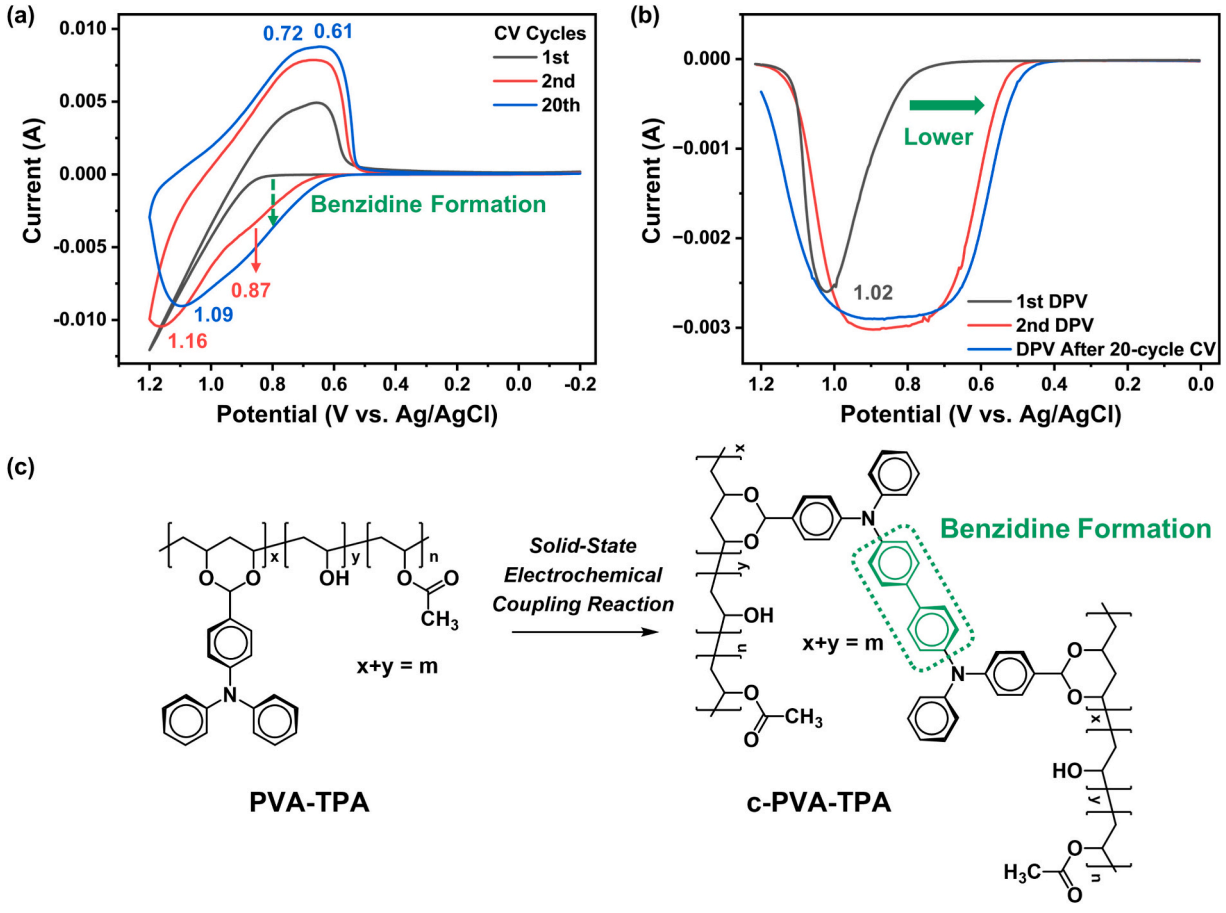

Fig. 2. (a) Solid-state electrochemical coupling test using cyclic voltammetry at a scan rate of 50 mV/s. (b) Differential pulse voltammetric profiles from 0.0 to 1.2 V at an increment of 4 mV, pulse width of 25 ms, pulse period of 0.2 s, and pulse amplitude of 50 mV. All the electrochemical measurements were conducted in 0.1 M $TBABF_4$/MeCN and 1 × 1 cm^2 of platinum plate as the counter electrode. (c) Schematic presentation of the solid-state electrochemical coupling reaction.

consequences also occurred: only one oxidation peak was observed at the first scan at 1.02 V, attributed to the oxidation reaction of the TPA moiety; a broad and low oxidation peak at the second DPV scan appeared, as depicted in Fig. 2b. When the CV scans increased to twenty cycles, the shape of the CV profiles became steady and showed no noticeable change in the current (Fig. S7). The resulting polymer film is

seen as fully transformed to the TPB structure, suggested as a cross-linked conformation (Fig. 2c), named c-PVA-TPA. The resulting DPV profile of c-PVA-TPA displayed a broad oxidation peak from 0.50 V to 1.20 V, and the reversible DPV profile exhibited two reduction peaks that merged at 1.04 V and 0.91 V (Fig. S8). Similarly, the CV profile revealed a clear oxidation potential at 1.09 V with two reduction couples at 0.72 V and 0.61 V owing to the weak electron-coupling ability between the two electroactive nitrogen atoms in the TPB moiety.

In addition to the electrochemical characteristic changes, UV–vis-NIR spectroscopy was also utilized to investigate the optical behaviors of structural transformation. As illustrated in Fig. 3a, before the coupling reaction, the onset wavelength (λ_{onset}) was at 348 nm, and the distinct π–π* transition of the TPA moiety appeared at 311 nm. After the coupling reaction, the λ_{onset} was significantly bathochromic to 403 nm, suggesting a smaller bandgap (E_g^{Opt}) value of 3.08 eV than that of PVA-TPA (3.56 eV). A new absorption peak appeared at 356 nm, attributed to the TPB moiety's π–π* transition. Note that the main absorption after the coupling reaction was located in the UV region, making the resulting c-PVA-TPA still reveal a highly transparent and colorless appearance. To confirm the formation of the cross-linking structure we supposed, the polymer films were coated on ITO glasses and immersed in concentrated sulfuric acid (H_2SO_4) before or after the electrochemical coupling reaction to observe the solubility difference. In Fig. 3a, the PVA-TPA film was completely dissolved in the concentrated H_2SO_4 with a yellow color, leaving only the ITO glass substrate in the vial. On the other hand, the c-PVA-TPA film could only peel off from the ITO glass substrate and float in the concentrated H_2SO_4 instead of being dissolved in it, demonstrating the cross-linked structure of c-PVA-TPA. Intriguingly, the color, whether the PVA-TPA solution or the c-PVA-TPA film in the concentrated H_2SO_4, would change to a yellow or orange appearance because the TPA or TPB moieties could undergo the chemical oxidative reaction in the presence of the concentrated H_2SO_4.

2.3. Electrochromic behaviors of c-PVA-TPA

The PVA-TPA and c-PVA-TPA films coated onto ITO glass substrates were analyzed using the spectroelectrochemical technique to evaluate their electrochromic behaviors. The c-PVA-TPA films were prepared after twenty cycles of CV scans from PVA-TPA and measured directly without further purification. For comparison, a structure-related TPB-PA was utilized (Scheme 2), and the corresponding CV diagram was depicted in Fig. S9. First, the pristine PVA-TPA film was used to observe the absorption changes during the coupling reaction with the different applied potentials in situ, and each applied potential was kept for two minutes to ensure reaching a steady state. In its neutral state, the PVA-TPA film appeared colorless and transparent with CIELAB values of $L^* = 98.10$, $a^* = 0.65$, and $b^* = 0.37$. Fig. 3b displays that the UV–vis-NIR spectra did not change when the applied potential was from 0 V to 0.90 V and exhibited the same profiles as the neutral state. Subsequently, the

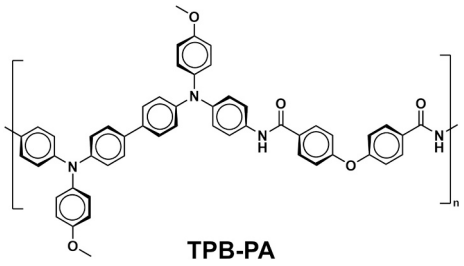

Scheme 2. Chemical structure of the conventional TPB-based polyamide, TPB-PA.

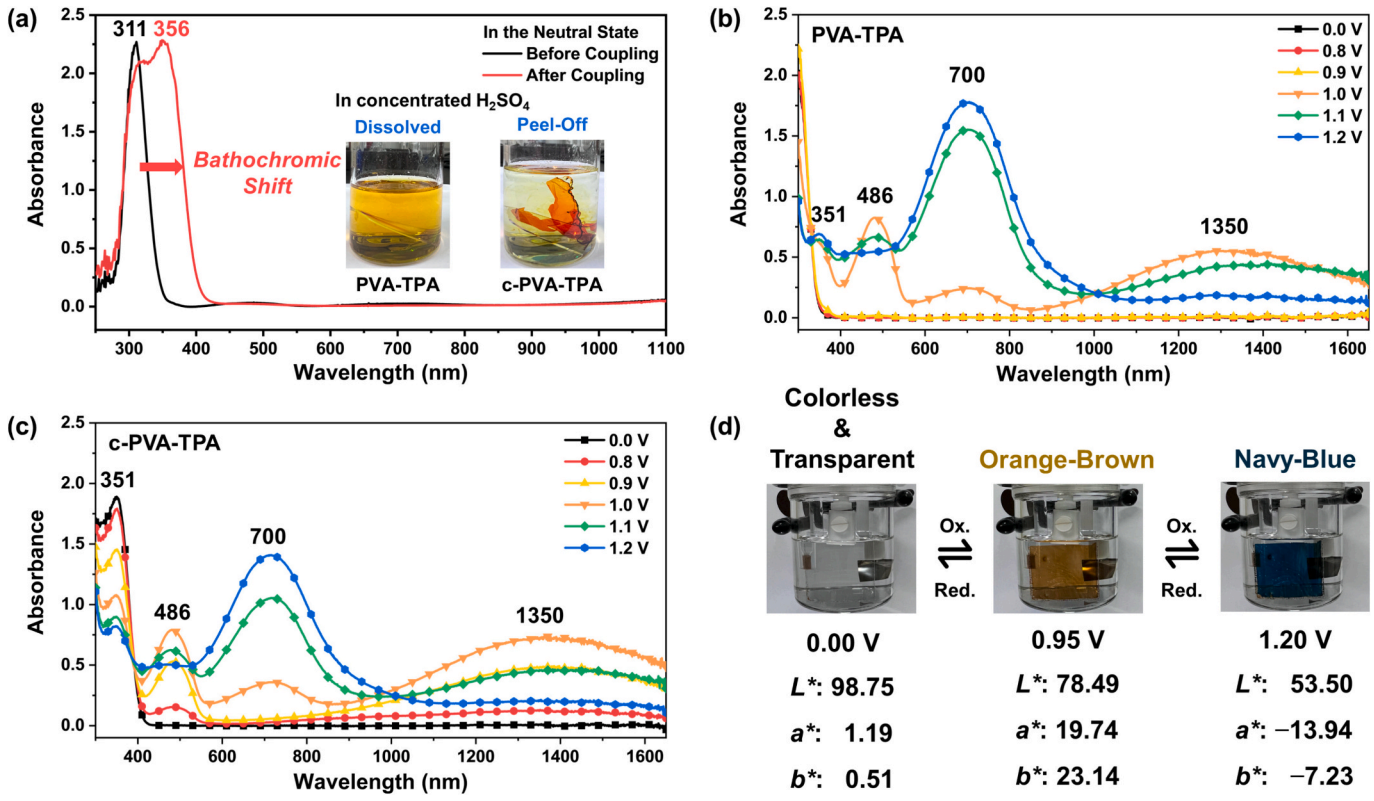

Fig. 3. (a) UV–vis-NIR spectra of the PVA-TPA and c-PVA-TPA films in the neutral state. The inserted photos were the PVA-TPA and c-PVA-TPA films immersed in concentrated sulfuric acid. Spectroelectrochemistry of (b) PVA-TPA and (c) c-PVA-TPA at different applied potentials in 0.1 M $TBABF_4$/MeCN and 1 × 1 cm^2 of platinum plate as the counter electrode; each applied potentials were kept for two minutes to ensure reaching the steady state. (d) Photos of the appearance of electrochromic behaviors for the c-PVA-TPA film.

characteristic absorption peaks emerged at 351 nm, 486 nm, 700 nm, and 1350 nm at 1.0 V, and the 700 nm absorption peak could increase further when raised to 1.20 V, while the absorption peaks at 486 and 1350 nm decreased gradually. The distinct absorption peak at 1350 nm could be distinguished as the mixed-valence (or intervalence charge transfer, IVCT) absorption of the TPB^{+} moiety caused by the charge delocalization between two redox centers and the biphenyl bridge in the first oxidation state. Thus, the fast structural transformation makes it difficult to observe the pristine absorption or chromic color of the oxidized TPA moiety. After the electrochemical coupling reaction, the c-PVA-TPA film also revealed a highly colorless and transparent appearance, with the CIELAB values being $L^* = 98.75$, $a^* = 1.19$, and $b^* = 0.51$.

In comparison, the conventional TPB-based polyamide (L^*, 93.47; a^*, −1.56; b*, 2.46) in the same thickness revealed a higher b^* value than that of the c-PVA-TPA film, resulting in a slightly yellowish film appearance. The optical spectra of c-PVA-TPA started changing at the low driving potential of 0.80 V, gradually generating the absorption peaks at 486 nm and 1350 nm and decreasing at 351 nm until 1.0 V, and the film appearance would change from colorless to orange-brown appearances (L^*, 78.49; a^*, 19.74; b*, 23.14) (Fig. 3c and d). When applying a further driving potential to 1.20 V, the distinct IVCT absorption would reduce owing to the fully oxidized TPB^{2+} moiety not being able to have mix-valence ability, and the absorbance at 700 nm would increase substantially to perform a navy-blue appearance (L^*, 53.50; a^*, −13.94; b*, −7.23). Thus, this approach could achieve the excellent processability of the PVA-TPA and preserve the original transparent and colorless features after the electrochemical coupling reaction, making c-PVA-TPA a gratifyingly promising EC material.

Subsequently, the EC behaviors of the resulting c-PVA-TPA were further investigated and compared to the structure-related TPB-PA. To reach 90% of ΔT% at 486 nm in the coloring process in the first oxidation stage, the c-PVA-TPA film needed 6.8 s with a coloration speed ($\nu_{c,\ 90\%}$) of 11.4% s^{-1}, which is comparable to the TPB-PA one that performed a 5.4-s coloring time (t_c) with a $\nu_{c,\ 90\%}$ of 14.0% s^{-1}, as depicted in Fig. 4a. If calculating to 95% of ΔT% in the coloring process, although c-PVA-TPA still required a longer coloration time ($t_{c,\ 95\%}$: 9.3 s) than TPB-PA ($t_{c,\ 95\%}$: 8.8 s), within this 5% of ΔT%, c-PVA-TPA required a shorter time of 2.5 s than that of TPB-PA (3.4 s), leading to comparable $\nu_{c,\ 95\%}$ values of c-PVA-TPA (8.8% s^{-1}) and TPB-PA (9.0% s^{-1}). Both c-PVA-TPA and TPB-PA displayed rapid bleaching capability with similar bleaching times (t_b, 90%) of 1.8 s in the bleaching process.

In the second oxidation stage, we monitored two different wavelengths of c-PVA-TPA at 486 and 700 nm. In Fig. S10, the transmittance changes at 486 and 700 nm revealed a longer $t_{c,\ 90\%}$ of 8.9 s, compared to that in the first oxidation stage, and a shorter $t_{b,\ 90\%}$ of 1.5 s. Furthermore, *Supporting Videos 1* and *2* presented that c-PVA-TPA performed remarkable color reversibility from colorless (neutral state) to brown appearance (first oxidation stage) or even to navy-blue appearance (second oxidation stage) and fast response capabilities.

In addition, different from the results of the response capability, the coloration efficiency (η_{CE}, $cm^2\ C^{-1}$) of c-PVA-TPA (199.8 $cm^2\ C^{-1}$) displayed a higher value than TPB-PA (171.4 $cm^2\ C^{-1}$) at 486 nm in the first oxidation stage, as illustrated in Fig. S11, indicating that c-PVA-TPA required less current consumption than TPB-PA at the same optical density and exhibited an energy-saving feature. To elucidate this phenomenon, electrochemical impedance spectroscopy (EIS) was applied to analyze the charge-transfer resistance (R_{ct}, Ω) and the diffusivity of the counter ions (D, $cm^2\ s^{-1}$) [49–51]. As shown in Figs. 4b and S12, both c-PVA-TPA and TPB-PA exhibited similar R_{ct} values of 35.9 Ω and 34.0 Ω in the first oxidation stage, indicating that the ability of the electron transfer was similar within these two materials; meanwhile, c-PVA-TPA had a ten times larger D value (45.2×10^{-15}) than TPB-PA (4.5×10^{-15}). We speculated that the polarity group in the c-PVA-TPA backbone (such as hydroxyl and ester groups) and the conformation via the electrochemical coupling reaction facilitated the migration of the counter ions within the polymer matrices, making c-PVA-TPA with a higher η_{CE} (199.8 $cm^2\ C^{-1}$) value than the structure-related TPB-PA (η_{CE} = 171.4 $cm^2\ C^{-1}$).

2.4. Electrochromic and Electrofluorochromic devices

To conduct the feasibility for the practical applications, c-PVA-TPA was further fabricated as the gel-type EC devices (ECD) using 0.1 M of $TBABF_4$ as the supporting electrolyte and 0.03 M of heptyl viologen (HV) as the counter cathodic EC material in the dry propylene carbonate (PC) with 10 wt% of PMMA. The CV profile of c-PVA-TPA revealed only one oxidation potential at 1.46 V (Fig. S13), but even so, the two corresponding reduction peaks at 1.18 V and 0.95 V still could be observed, similar to the case of the pristine film. For comparison, the CV profile and spectroelectrochemical spectra of the TPB-PA-based ECDs were also measured and provided in Figs. S14 and S15 to distinguish the exact first oxidation potential. As depicted in Fig. 5, the prepared c-PVA-TPA ECD did not show an apparent absorption in the visible region in the neutral state, displayed a colorless and transparent appearance, and could be activated at 1.10 V, then started gradually increasing absorption with distinct peaks at 486 and 1425 nm. The reduced HV's generated absorptions at 385, 605, 665, and 735 nm. When reaching 1.40 V, the

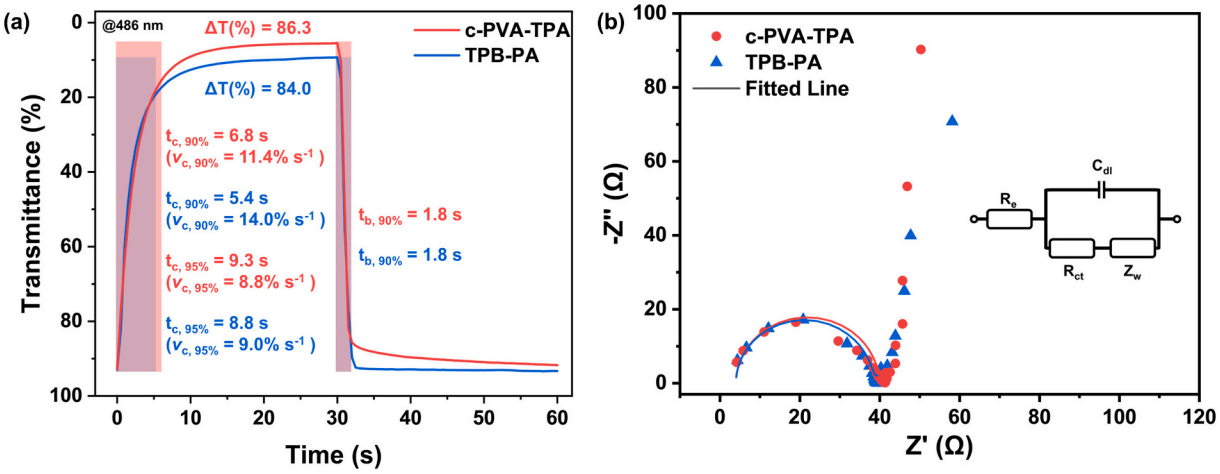

Fig. 4. (a) Response times of the c-PVA-TPA and TPB-PA films at 486 nm. (b) Electrochemical impedance spectroscopy of the c-PVA-TPA and TPB-PA films in the first oxidation state. (Inserted circuit is the Randles equivalent circuit, where R_e: electrolyte resistance; C_{dl}: double-layer capacitance; Z_w: Warburg resistance; R_{ct}: charge-transfer resistance).

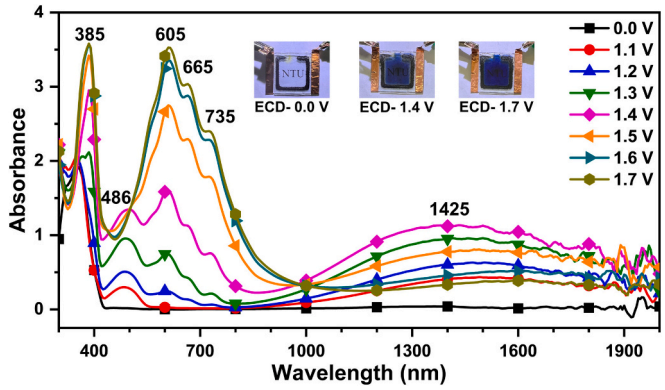

Fig. 5. Spectroelectrochemistry of c-PVA-TPA ECD at different applied potentials. (0.1 M of $TBABF_4$ as the supporting electrolyte and 0.03 M of heptyl viologen (HV) as the counter cathodic EC material in the dry propylene carbonate (PC) with 10 wt% of PMMA; active area: 2 × 2 cm^2).

peaks at 486 and 1425 nm exhibited a maximum absorbance value and a decrease after being applied to 1.50 V. Therefore, the potential of 1.40 V could be regarded as the end of the first oxidation potential of the c-PVA-TPA ECD. In the second oxidation stage, the distinct absorption at 700 nm of the fully oxidized c-PVA-TPA would be merged with the absorption of the reduced HV and display a broad absorption band from 500 to 1000 nm, revealing a deep blue appearance. As a reference, TPB-PA with the structure-related tetraphenylbenzidine-based electrochromic composition of c-PVA-TPA was also fabricated as the gel-type ECD to compare the EC behaviors. Fig. 6a and b reveal that c-PVA-TPA and TPB-PA performed similarly $t_{c,\ 90\%}$ values of 1.7 and 1.8 s, respectively. Interestingly, in the bleaching process, c-PVA-TPA ECD exhibited a quicker response time of $t_{b,\ 90\%}$ of 2.0 s, just half of the $t_{b,\ 90\%}$ for TPB-PA ECD (3.9 s). The results were different from the findings in the pristine films, suggesting that in the limited electrolyte system, the poly(vinyl acetal) structure could facilitate imparting a higher impact on the counter ion diffusion to generate a more significant difference in the bleaching process than the bulk electrolyte system. In addition, the η_{CE} of c-PVA-TPA also exhibited a larger value (360.5 $cm^2\ C^{-1}$) than the TPB-PA ECD (312.2 $cm^2\ C^{-1}$), as shown in Fig. 6c. In the long-term switching stability test, the c-PVA-TPA ECD also displayed a gratifying retention of up to 90% of ΔT% after 60,000 s (1,000 cycles); in comparison, TPB-PA ECD exhibited a retention of 96% stability (Fig. 6d and e). These findings confirm that the prepared c-PVA-TPA by this facile approach is low-cost and eco-friendly and could perform comparable or even superior EC properties to the conventional ones.

The TPA moiety usually shows non- or weakly emissive behaviors in the solid or film states, while it could perform highly emissive when functionalized appropriately. The TPB moiety demonstrated good photoluminescence (PL) properties in the family of TPA derivatives in the solid and film states [52,53]. Hence, the c-PVA-TPA might be expected to show emissive behavior in the film state and be applied in electrofluorochromism (EFC). First, we investigate the PL properties of the original PVA-TPA in the various organic solvents. As shown and listed in Fig. S16 and Table S5, PVA-TPA revealed similar maximum absorption wavelengths around 300 nm in the different organic solvents, attributed to the π-π* transition of the TPA moiety. Subsequently, two emission peaks emerged at 367 nm and 440 nm for all cases in the emission spectra, where the former one could be attributed to the distinct emission of the TPA moiety, and the latter might result from the excimer formation or aggregation of TPA moieties [54,55]. The solution-state relative quantum efficiency (Φ_{QY}) values also exhibited the low energy

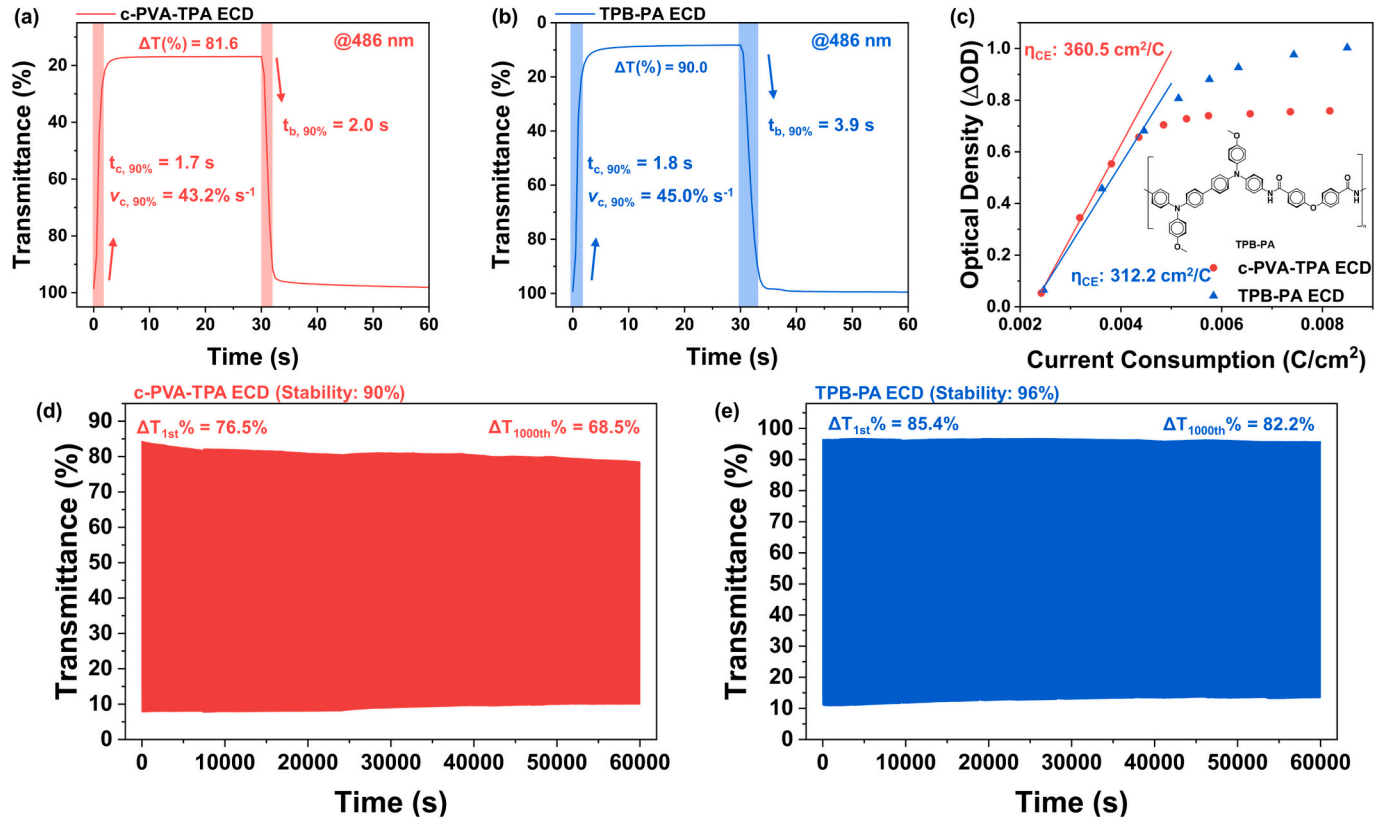

Fig. 6. Response times of (a) c-PVA-TPA ECD and (b) TPB-PA ECD at 486 nm. (c) Plots of the optical density at 486 nm versus current consumption and slopes are defined and calculated as coloration efficiency. Switching stabilities of (d) c-PVA-TPA ECD and (e) TPB-PA ECD at 486 nm for 1000 cycles (cycle time: 60 s). (0.1 M of $TBABF_4$ as the supporting electrolyte and 0.03 M of heptyl viologen (HV) as the counter cathodic EC material in the dry propylene carbonate (PC) with 10 wt% of PMMA; active area: 2 × 2 cm^2).

conversion, with only 2.0% to 4.8% and without significant changes, resulting from the intramolecular motions causing the emission quenching. As in the film, the photograph of PVA-TPA taken under UV 365-nm irradiation displayed blue emissive behavior; nevertheless, the c-PVA-TPA film after the electrochemical coupling reaction exhibited highly green emissive behavior, as shown in Fig. 7a. Thus, the EFC characteristic of the c-PVA-TPA device was evaluated, and the composition of the c-PVA-TPA EFC device (EFCD) was the same as the c-PVA-TPA ECD. In the neutral state, the c-PVA-TPA EFCD revealed a broad emission peak around 500 nm, and the intensity decreased dramatically at 1.10 V, indicating a high response in the emission intensity under the applied potential. Finally, the emission intensity would be quenched at 1.40 V with an intensity contrast ratio of 34.6, as illustrated in Fig. 7b. *Supporting Video 3* presents that the resulting EFCD displayed rapid emission quenching and reversibility behavior during the redox process. In summary, we demonstrate that TPA-containing poly(vinyl acetal) electrode material, after a solid-state electrochemical coupling reaction, could be applied not only in the EC application with comparable properties to the structure-related conventional TPB-PA but also in the EFC application with a gratifying intensity contrast ratio.

3. Conclusion

In this study, a low-cost and eco-friendly facile approach for preparing EC materials was judiciously designed and developed. The acetalization of PVA with 4-formyltriphenylamine was performed at a mild reaction temperature (60 °C) using a non-toxic acid catalyst (*p*-TSA) and the green, less-toxic solvent DMSO. The resulting PVA-TPA polymer achieved a respectable acetalization degree of 63.3% with high thermal stability. A solid-state electrochemical coupling reaction via CV scanning was employed for EC electrode preparation, gratifyingly transforming the TPA into TPB moieties without wasting starting materials and requiring additional purification processes for the pristine film preparation or during ECD fabrication. The prepared c-PVA-TPA film demonstrated EC performance comparable to, or even better than, the structure-related polyamide of TPB-PA, offering similar response capabilities and a higher η_{CE} value. Additionally, the c-PVA-TPA ECD exhibited superior response capabilities ($t_{c,\ 90\%} = 1.7$ s, $t_{b,\ 90\%} = 2.0$ s) and higher η_{CE} (360.5 $cm^2\ C^{-1}$) values than the TPB-PA ECD ($t_{c,\ 90\%} = 1.8$ s, $t_{b,\ 90\%} = 3.9$ s, $\eta_{CE} = 312.2\ cm^2\ C^{-1}$), along with excellent switching stability. Beyond EC applications, c-PVA-TPA also displayed EFC features, achieving an intensity contrast ratio of 34.6. These features open scalable application pathways in areas such as smart architectural and automotive glazing (multi-level solar/IR modulation), anti-counterfeiting and encrypted dual-mode (color and fluorescence changes) security elements, wearable or environmental visual indicators, underscoring the universality, sustainability, and translational potential of this approach. In conclusion, these findings highlight the facile, eco-friendly, cost-effective, and scalable multifunctional material potential for emerging practical applications.

4. Experimental section

4.1. Preparation of TPA-containing poly(vinyl acetal)

Partial hydrolysis PVA (BP-17, M_w: 84,000–89,000; hydrolysis degree: 86% ~ 89%) and DMSO were added into a 50-mL flask and heated to 100 °C. After PVA dissolved and cooled down to 60 °C, p-TSA and 4-formyltriphenylamine were added with an equivalent ratio of 0.6 and 0.1 (compared to the hydroxy groups of PVA). The reaction was stirred for four hours, and the solution was precipitated into water to afford a fiber-like precipitate. The crude product was undergoing Soxhlet extraction with MeOH overnight. The pale gray product (PVA-TPA) was dried in the vacuum oven at 80 °C for one day.

4.2. Film preparation and oxidative coupling reaction

PVA-TPA was dissolved in DMAc with a concentration of 2.0 mg mL^{-1}, and 400 μL of the solution was drop-coated on a 30 × 25 mm^2 area of ITO-coated glass (AimCore Technology Co., Ltd., 7 Ω), then the solvent was removed in the vacuum oven, as depicted in Scheme S2. The prepared polymer electrode with a size of 5 × 25 mm^2 polymer film underwent an oxidative coupling reaction to form a cross-linked PVA-TPA (cPVA-TPA) polymer film (The film-state electrochemical measurements were all in the three-electrode electrochemical cell using 0.1 M $TBABF_4$ in acetonitrile as the electrolyte, Ag/AgCl as the reference electrode, and 10 × 10 mm^2 of Pt plate as the counter electrode) for the film-state electrochemical measurements without further purification process.

Supporting information

Coloration efficiency of the polymer film, thermal properties, solubilities, electrochemical measurements, photoluminescence spectra of

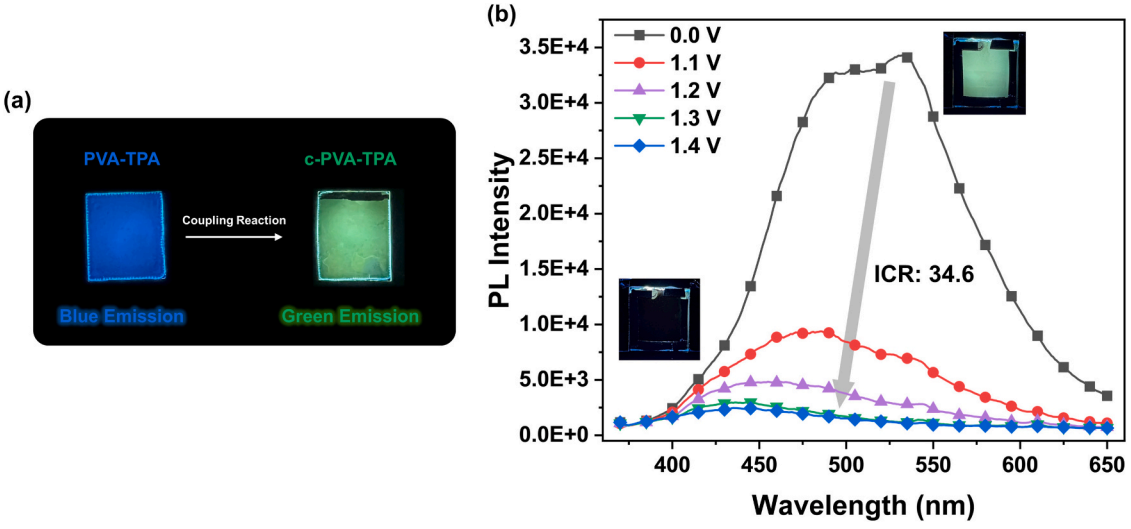

Fig. 7. (a) Photographs of the PVA-TPA and c-PVA-TPA films under UV 365-nm irradiation. (b) Photoluminescence spectra of c-PVA-TPA EFCD at different applied potentials, irradiated at 356 nm. (0.1 M of $TBABF_4$ as the supporting electrolyte and 0.03 M of heptyl viologen (HV) as the counter cathodic EC material in the dry propylene carbonate (PC) with 10 wt% of PMMA; active area: 2 × 2 cm^2).

the PVA-TPA in the solution state, and the calculation method for the diffusion coefficient.

Supplementary data to this article can be found online at https://doi.org/10.1016/j.susmat.2025.e01703.

CRediT authorship contribution statement

Yu-Jen Shao: Writing – original draft, Visualization, Validation, Methodology, Investigation, Formal analysis. **Chin-Hsuan Lin:** Investigation, Formal analysis. **Toshifumi Satoh:** Writing – review & editing, Supervision. **Cha-Wen Chang:** Writing – review & editing, Project administration, Conceptualization. **Guey-Sheng Liou:** Writing – review & editing, Supervision, Project administration, Funding acquisition, Data curation, Conceptualization.

Funding

This work was supported by the Japan Science and Technology Agency (JST) SPRING (Grant number: JPMJSP2119) and the National Science and Technology Council in Taiwan (NSTC 113–2221-E-002-061-MY3 and 111–2221-E-002-028-MY3).

Declaration of competing interest

The authors declare that they have no known competing financial interests or personal relationships that could have appeared to influence the work reported in this paper.

Acknowledgment

This work was supported by JST SPRING, Grant Number JPMJSP2119, and the National Science and Technology Council in Taiwan (NSTC 113-2221-E-002-061-MY3 and 111-2221-E-002-028-MY3).

Data availability

The data that has been used is confidential.

References

[1] H. Meng, Organic Electronics for Electrochromic Materials and Devices, John Wiley & Sons, 2021.
[2] K. Madasamy, D. Velayutham, V. Suryanarayanan, M. Kathiresan, K.-C. Ho, Viologen-based electrochromic materials and devices, J. Mater. Chem. C 7 (16) (2019) 4622–4637.
[3] G.K. Pande, J.S. Heo, J.H. Choi, Y.S. Eom, J. Kim, S.K. Park, J.S. Park, RGB-to-black multicolor electrochromic devices enabled with viologen functionalized polyhedral oligomeric silsesquioxanes, Chem. Eng. J. 420 (2021) 130446.
[4] L. Cheng, W. Luo, Y. Liu, X. Zeng, X. Yu, Y. Zhang, Electrochromism and Bistable electrochromic devices of five-membered-heterocycle bridged viologen polymers, ACS Appl. Polym. Mater. 6 (14) (2024) 8191–8199.
[5] J. Guo, H. Jia, Z. Shao, P. Jin, X. Cao, Fast-switching WO3-based electrochromic devices: design, fabrication, and applications, Acc. Mater. Res. 4 (5) (2023) 438–447.
[6] A. Kraft, Too blue to be good? A critical overview on the electrochromic properties and applications of Prussian blue, Sol. Energy Mater. Sol. Cells 278 (2024) 113195.
[7] Y. Ding, H. Sun, Z. Li, C. Jia, X. Ding, C. Li, J.-G. Wang, Z. Li, Galvanic-driven deposition of large-area Prussian blue films for flexible battery-type electrochromic devices, J. Mater. Chem. A 11 (6) (2023) 2868–2875.
[8] X. Fu, K. Li, C. Zhang, Q. Wang, G. Xu, A.A. Rogachev, M.A. Yarmolenko, H. Cao, H. Zhang, Homogeneous and Nanogranular Prussian blue to enable long-term-stable electrochromic devices, ACS Appl. Mater. Interfaces 16 (14) (2024) 17745–17756.
[9] H. Li, J. Cao, F. Liu, W. Zhou, X. Chen, Y. Deng, Z. Wu, B. Lu, D. Mo, J. Xu, Stable three-dimensional PEDOT network construction for electrochromic-supercapacitor dual functional application, ACS Appl. Energy Mater. 5 (10) (2022) 12315–12323.
[10] Lv, H.; Wei, Z.; Han, C.; Yang, X.; Tang, Z.; Zhang, Y.; Zhi, C.; Li, H. Cross-linked polyaniline for production of long lifespan aqueous iron|| organic batteries with electrochromic properties. Nat. Commun. 2023, 14 (1), 3117.
[11] D. Zhang, J. Wang, Z. Tong, H. Ji, H.Y. Qu, Bioinspired dynamically switchable PANI/PS-b-P2VP thin films for multicolored electrochromic displays with long-term durability, Adv. Funct. Mater. 31 (45) (2021) 2106577.
[12] H.-J. Yen, G.-S. Liou, Design and preparation of triphenylamine-based polymeric materials towards emergent optoelectronic applications, Prog. Polym. Sci. 89 (2019) 250–287.
[13] C. Lambert, G. Nöll, The class II/III transition in triarylamine redox systems, J. Am. Chem. Soc. 121 (37) (1999) 8434–8442.
[14] H.J. Yen, S.M. Guo, G.S. Liou, J.C. Chung, Y.C. Liu, Y.F. Lu, Y.Z. Zeng, Mixed-valence class I transition and electrochemistry of bis (triphenylamine)-based aramids containing isolated ether-linkage, J. Polym. Sci. A Polym. Chem. 49 (17) (2011) 3805–3816.
[15] C. Gu, A.-B. Jia, Y.-M. Zhang, S.X.-A. Zhang, Emerging electrochromic materials and devices for future displays, Chem. Rev. 122 (18) (2022) 14679–14721.
[16] J.H. Wu, G.S. Liou, High-performance Electrofluorochromic devices based on electrochromic and Photoluminescent-active novel poly(4-Cyanotriphenylamine), Adv. Funct. Mater. 24 (41) (2014) 6422–6429.
[17] M. Aslam, M.A. Kalyar, Z.A. Raza, Polyvinyl alcohol: a review of research status and use of polyvinyl alcohol based nanocomposites, Polym. Eng. Sci. 58 (12) (2018) 2119–2132.
[18] S.G. Jin, Production and application of biomaterials based on polyvinyl alcohol (PVA) as wound dressing, Chem. Asian J. 17 (21) (2022) e202200595.
[19] X. Li, H. Xu, W. Yan, Preparation and characterization of PbO 2 electrodes modified with polyvinyl alcohol (PVA), RSC Adv. 6 (85) (2016) 82024–82032.
[20] P.B. Pawar, S. Shukla, S. Saxena, Graphene oxide–polyvinyl alcohol nanocomposite based electrode material for supercapacitors, J. Power Sources 321 (2016) 102–105.
[21] J. Zhang, L. Wan, Y. Gao, X. Fang, T. Lu, L. Pan, F. Xuan, Highly stretchable and self-healable MXene/polyvinyl alcohol hydrogel electrode for wearable capacitive electronic skin, Adv. Electron. Mater. 5 (7) (2019) 1900285.
[22] L. Ding, N. Yan, S. Zhang, R. Xu, T. Wu, F. Yang, Y. Cao, M. Xiang, Separator impregnated with polyvinyl alcohol to simultaneously improve electrochemical performances and compression resistance, Electrochim. Acta 403 (2022) 139568.
[23] Y. Xia, X. Li, J. Zhuang, Y. Yuan, W. Wang, Cellulose microspheres enhanced polyvinyl alcohol separator for high-performance lithium-ion batteries, Carbohydr. Polym. 300 (2023) 120231.
[24] W. Xiao, L. Zhao, Y. Gong, J. Liu, C. Yan, Preparation and performance of poly (vinyl alcohol) porous separator for lithium-ion batteries, J. Membr. Sci. 487 (2015) 221–228.
[25] Y. Qin, F. Yang, J.A. Yuwono, A. Varzi, Dehydroxylated polyvinyl alcohol separator enables fast kinetics in zinc-metal batteries, Small 2410758 (2025).
[26] F. Chabert, D.E. Dunstan, G.V. Franks, Cross-linked polyvinyl alcohol as a binder for gelcasting and green machining, J. Am. Ceram. Soc. 91 (10) (2008) 3138–3146.
[27] J. He, L. Zhang, Polyvinyl alcohol grafted poly (acrylic acid) as water-soluble binder with enhanced adhesion capability and electrochemical performances for Si anode, J. Alloys Compd. 763 (2018) 228–240.
[28] P. Mandal, K. Stokes, G. Hernández, D. Brandell, J. Mindemark, Influence of binder crystallinity on the performance of Si electrodes with poly (vinyl alcohol) binders, ACS Appl. Energy Mater. 4 (4) (2021) 3008–3016.
[29] B.R.S. Reddy, J.-H. Ahn, H.-J. Ahn, G.-B. Cho, K.-K. Cho, Low-Cost and Sustainable Cross-Linked Polyvinyl Alcohol–Tartaric Acid Composite Binder for High-Performance Lithium–Sulfur Batteries, ACS Appl. Energy Mater. 6 (11) (2023) 6327–6337.
[30] A.F. Fitzhugh, R.N. Crozier, Relation of composition of polyvinyl acetals to their physical properties. I. Acetals of saturated aliphatic aldehydes, J. Polym. Sci. 8 (2) (1952) 225–241.
[31] T.P. Blomstrom, Polyvinyl acetal resins, Coat. Technol. Handb. 60 (61–60) (2005) 11.
[32] C. Carrot, A. Bendaoud, C. Pillon, O. Olabisi, K. Adewale, Polyvinyl butyral, Handb. Thermoplast. 2 (2016) 89–137.
[33] X. Zhang, H. Hao, Y. Shi, J. Cui, The mechanical properties of polyvinyl Butyral (PVB) at high strain rates, Constr. Build. Mater. 93 (2015) 404–415.
[34] J. Huntsberger, Adhesion of plasticized polyvinyl butyral to glass, J. Adhes. 13 (2) (1981) 107–129.
[35] X. Wang, Y. Yang, Q. Jin, Q. Lou, Q. Hu, Z. Xie, W. Song, A scalable, robust polyvinyl-Butyral-based solid polymer electrolyte with outstanding ionic conductivity for laminated large-area WO3–NiO electrochromic devices, Adv. Funct. Mater. 33 (30) (2023) 2214417.
[36] D. Rong, Y. Wu, W. Wang, X. Shang, S. Wang, S. Wang, Polyvinyl Butyral solid electrolyte film and its electrochromic laminated safety glass, ACS Appl. Mater. Interfaces 16 (47) (2024) 65394–65401.
[37] X. Zhang, J. Wang, D. Hu, W. Du, C. Hou, H. Jiang, Y. Wei, X. Liu, F. Jiang, J. Sun, High-performance lithium metal batteries based on composite solid-state electrolytes with high ceramic content, Energy Storage Mater. 65 (2024) 103089.
[38] F. Lian, Y. Wen, Y. Ren, H. Guan, A novel PVB based polymer membrane and its application in gel polymer electrolytes for lithium-ion batteries, J. Membr. Sci. 456 (2014) 42–48.
[39] S. Zhao, W. Huang, Z. Guan, B. Jin, D. Xiao, A novel bis (dihydroxypropyl) viologen-based all-in-one electrochromic device with high cycling stability and coloration efficiency, Electrochim. Acta 298 (2019) 533–540.
[40] S. Pal, D. Das, S. Bhunia, p-Toluenesulfonic acid-promoted organic transformations for the generation of molecular complexity, Org. Biomol. Chem. 22 (8) (2024) 1527–1579.
[41] W. Xie, T. Li, C. Chen, H. Wu, S. Liang, H. Chang, B. Liu, E. Drioli, Q. Wang, J. C. Crittenden, Using the green solvent dimethyl sulfoxide to replace traditional solvents partly and fabricating PVC/PVC-g-PEGMA blended ultrafiltration membranes with high permeability and rejection, Ind. Eng. Chem. Res. 58 (16) (2019) 6413–6423.

[42] M. Wang, X. Dong, I.C. Escobar, Y.-T. Cheng, Lithium ion battery electrodes made using dimethyl sulfoxide (DMSO)—a green solvent, ACS Sustain. Chem. Eng. 8 (30) (2020) 11046–11051.
[43] M. Rostagno, S. Shen, I. Ghiviriga, S.A. Miller, Sustainable polyvinyl acetals from bioaromatic aldehydes, Polym. Chem. 8 (34) (2017) 5049–5059.
[44] Y.-K. Su, C.M. Coxwell, S. Shen, S.A. Miller, Polyvinyl alcohol modification with sustainable ketones, Polym. Chem. 12 (34) (2021) 4961–4973.
[45] G.S. Liou, H.Y. Lin, Synthesis and electrochemical properties of novel aromatic poly(amine−amide)s with Anodically highly stable yellow and blue electrochromic behaviors, Macromolecules 42 (1) (2009) 125–134.
[46] H.J. Yen, K.Y. Lin, G.S. Liou, Transmissive to black electrochromic aramids with high near-infrared and multicolor electrochromism based on electroactive tetraphenylbenzidine units, J. Mater. Chem. 21 (17) (2011) 6230–6237.
[47] Q. Huang, J. Chen, X. Shao, L. Zhang, Y. Dong, W. Li, C. Zhang, Y. Ma, New electropolymerized triphenylamine polymer films and excellent multifunctional electrochromic energy storage system materials with real-time monitoring of energy storage status, Chem. Eng. J. 461 (2023) 141974.
[48] S.-H. Hsiao, Y.-Z. Chen, Electrosynthesis of redox-active and electrochromic polymer films from triphenylamine-cored star-shaped molecules end-capped with arylamine groups, Eur. Polym. J. 99 (2018) 422–436.
[49] A. Eftekhari, The mechanism of ultrafast supercapacitors, J. Mater. Chem. A 6 (7) (2018) 2866–2876.
[50] M.D. Levi, V. Dargel, Y. Shilina, D. Aurbach, I.C. Halalay, Impedance spectra of energy-storage electrodes obtained with commercial three-electrode cells: some sources of measurement artefacts, Electrochim. Acta 149 (2014) 126–135.
[51] Y.-J. Shao, T.-C. Yen, C.-C. Hu, G.-S. Liou, Non-conjugated triarylamine-based intrinsic microporous polyamides for an electrochromic supercapacitor: diffusion dynamics and charge–discharge studies, J. Mater. Chem. A 11 (4) (2023) 1877–1885.
[52] J. Mei, N.L. Leung, R.T. Kwok, J.W. Lam, B.Z. Tang, Aggregation-induced emission: together we shine, united we soar!, Chem. Rev. 115 (21) (2015) 11718–11940.
[53] H.-T. Lin, J.-T. Wu, M.-H. Chena, G.-S. Liou, Novel electrochemical devices with high contrast ratio and response capability of electrochromic and Electrofluorochromic Behaviours simultaneously, J. Mater. Chem. C 6 (5) (2018).
[54] W.Z. Yuan, Y. Gong, S. Chen, X.Y. Shen, J.W. Lam, P. Lu, Y. Lu, Z. Wang, R. Hu, N. Xie, Efficient solid emitters with aggregation-induced emission and intramolecular charge transfer characteristics: molecular design, synthesis, photophysical behaviors, and OLED application, Chem. Mater. 24 (8) (2012) 1518–1528.
[55] M. Shibano, M. Karakawa, H. Kamitakahara, T. Takano, Preparation and electro-optical properties of triphenylamine-bound chitosan derivative, Int. J. Biol. Macromol. 126 (2019) 1112–1115.